



This is a repository copy of *An arbitrary-order continuous sliding mode control technique for nonlinear PWR-type nuclear power plants*.

White Rose Research Online URL for this paper:

<https://eprints.whiterose.ac.uk/188616/>

Version: Accepted Version

Article:

Surjagade, P., Deng, J., Vajpayee, V. orcid.org/0000-0003-1179-7118 et al. (3 more authors) (2022) An arbitrary-order continuous sliding mode control technique for nonlinear PWR-type nuclear power plants. *Progress in Nuclear Energy*, 150. 104309. ISSN 0149-1970

<https://doi.org/10.1016/j.pnucene.2022.104309>

Article available under the terms of the CC-BY-NC-ND licence (<https://creativecommons.org/licenses/by-nc-nd/4.0/>).

Reuse

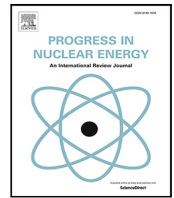
This article is distributed under the terms of the Creative Commons Attribution-NonCommercial-NoDerivs (CC BY-NC-ND) licence. This licence only allows you to download this work and share it with others as long as you credit the authors, but you can't change the article in any way or use it commercially. More information and the full terms of the licence here: <https://creativecommons.org/licenses/>

Takedown

If you consider content in White Rose Research Online to be in breach of UK law, please notify us by emailing eprints@whiterose.ac.uk including the URL of the record and the reason for the withdrawal request.



eprints@whiterose.ac.uk
<https://eprints.whiterose.ac.uk/>



An arbitrary-order continuous sliding mode control technique for nonlinear PWR-type nuclear power plants

Piyush V. Surjagade^{a,*}, Jiamei Deng^{a,*}, Vineet Vajpayee^b, Victor M. Becerra^c, S.R. Shimjith^{d,e}, A. John Arul^f

^a School of Built Environment, Engineering and Computing, Leeds Beckett University, Leeds, LS6 3QR, United Kingdom

^b Department of Automatic Control and Systems Engineering, The University of Sheffield, S10 2TN, United Kingdom

^c School of Energy and Electronic Engineering, University of Portsmouth, Portsmouth, PO1 3DJ, United Kingdom

^d Reactor Control Division, Bhabha Atomic Research Centre, Mumbai, 400 085, India

^e Homi Bhabha National Institute, Mumbai, 400 094, India

^f Probabilistic Safety, Reactor Shielding and Nuclear Data Section, Indira Gandhi Centre for Atomic Research, Kalpakkam, 603 102, India

ARTICLE INFO

Keywords:

Sliding mode control
Super-twisting algorithm
Large-scale System
Nuclear power reactor

ABSTRACT

This paper presents an arbitrary order continuous-time sliding mode controller based on the super-twisting algorithm for a nonlinear pressurized water nuclear power plant. A proportional-derivative terminal sliding surface is designed to achieve the finite time convergence and to enhanced the tracking performance. The proposed controller is chattering free, which is always preferable in most of the practical applications and, it is robust against Lipschitz in time uncertainties. The implementation of the proposed controller requires only the information about the system output, and thus, it is most suitable for large scale complex systems, such as nuclear power plants. Superiority of the proposed controller over some conventional control techniques in the presence of uncertainties is shown with the help of simulation results in the MATLAB/Simulink environment.

1. Introduction

Considering limited fossil fuel resources, an increase in day-by-day energy consumption, the recent energy crises around the world, and the harmful effects of global warming, the various types of sustainable energy sources such as nuclear, hydro, wind, solar, etc., are now gaining much-needed attention of academicians, manufacturers, governments, policy-makers, and the public. Among these sustainable energies, nuclear energy is undoubtedly a promising alternative resource. A facility designed to convert nuclear energy into electricity is called a Nuclear Power Plant (NPP). An NPP is a complex nonlinear system, where the system parameters vary with fuel burn-up, internal reactivity feedbacks, and with change in the power level and operating conditions. In addition to this, NPPs are often affected by uncertainties due to unmodelled dynamics, external disturbances, and ageing effects. The conventional control strategies fail to maintain the desired performance in such situations especially when the nature of uncertainties and disturbances is unknown. Thus, advanced robust control strategies are preferred over conventional approaches.

Sliding Mode Control (SMC) technique is one of the robust control techniques which is gaining considerable attention among researchers

because of its inherent robustness against uncertainties, simple structure, ease of implementation, and capability to effectively control both linear as well as nonlinear systems (Edwards and Spurgeon, 1998). Recently, different SMC strategies have been successfully applied to the control of NPPs (Vajpayee et al., 2020a; Desai et al., 2020; Patre et al., 2015; Zare Davijani et al., 2017; Abdulraheem and Korolev, 2021; Mostafavi and Ansarifar, 2021; Munje et al., 2016; Huang et al., 2004; Ansarifar, 2016). Vajpayee et al. (2020a) designed a robust subspace predictive control for a Pressurized Water Reactor (PWR) by combing a subspace-based predictive control with an integral SMC. Desai et al. (2020) and Patre et al. (2015) proposed an integral SMC and a fuzzy SMC for spatial power control of advanced heavy water reactor, respectively. Zare Davijani et al. (2017) proposed a fractional-order SMC for output power control of a research reactor based on nonlinear reduced-order fractional-order model. A hybrid optimal controller combining linear quadratic Gaussian/loop transfer recovery and integral SMC for a PWR operating in the load-following mode has been proposed in Abdulraheem and Korolev (2021). Mostafavi and Ansarifar (2021) proposed an observer-based dynamic SMC using Lyapunov-approach for level control of pressurizer in PWR type NPP. In Munje

* Corresponding authors.

E-mail addresses: p.surjagade@leedsbeckett.ac.uk (P.V. Surjagade), j.deng@leedsbeckett.ac.uk (J. Deng), v.vajpayee@sheffield.ac.uk (V. Vajpayee), victor.becerra@port.ac.uk (V.M. Becerra), srshim@barc.gov.in (S.R. Shimjith), arul@igcar.gov.in (A.J. Arul).

et al. (2016), a discrete-time sliding mode control is proposed for spatial power stabilization of advanced heavy water reactor. To design the controller the system is first linearized and decomposed into three subsystems by direct block diagonalization and then the control law is designed using only the slow subsystem states. Huang et al. (2004) proposed a multi-input multi-output fuzzy-adapted recursive sliding-mode controller for an advanced boiling water reactor NPP, to control reactor pressure, reactor water level and turbine power. In Ansarifar (2016), an adaptive dynamic sliding mode controller is proposed for the level control problem of U-tube nuclear steam generator considering the non-linear steam generator model which is developed based on the fundamental conservation equations for mass, energy and momentum.

Generally, an SMC is insensitive to parameter variations and can reject the disturbances entering through the input channel called matched disturbances. It is achieved through the discontinuous nature of the control action, which switches between the two distinctively different structures about a predefined sliding surface (Kamal et al., 2014). However, this discontinuity leads to high-frequency switching known as chattering, which is not desirable in practical systems. In literature, numerous methods are proposed to avoid the chattering phenomena (Utkin et al., 2009). A simple way to avoid high-frequency switching is by approximating the discontinuous function by its continuous counterpart like saturation function, sigmoid function, tanh function, etc. However, owing to such approximations, the disturbance rejection capability of an SMC is deteriorates (Utkin et al., 2009). The controllers proposed in Vajpayee et al. (2020a), Desai et al. (2020), Patre et al. (2015), Zare Davijani et al. (2017), Abdurhaheem and Korolev (2021) and Mostafavi and Ansarifar (2021) employ continuous-time approximation of discontinuous signum function to avoid the chattering. On the other hand, a more efficient way to avoid chattering without degrading the system performance and robustness is by designing higher-order SMC (Utkin et al., 2009). Among higher-order SMC techniques, Super Twisting Algorithm (STA) (Levant, 1993; Moreno and Osorio, 2012) is one of the most widely used second-order sliding mode algorithms. It is proposed for a sliding surface having a relative degree one. STA reduces the chattering significantly by generating continuous control input and at the same time retains all the properties of a conventional first-order SMC.

In the literature, STA-based observers as well as controllers have been effectively applied to the problem of nuclear reactor (Zahedi yeganeh and Ansarifar, 2018; Qaiser et al., 2009; Ansarifar and Rafiei, 2015; Hui et al., 2020; Abdurhaheem et al., 2021; Surjagade et al., 2020). In Zahedi yeganeh and Ansarifar (2018), authors proposed a higher order sliding mode observer based on STA to estimate the xenon and samarium concentration in PWR nuclear reactor considering the multi-point reactor model. In Qaiser et al. (2009) and Ansarifar and Rafiei (2015), authors proposed STA-based controllers to regulate the output power of a research reactor. Both the works focus on the similar problem, except the work proposed in Ansarifar and Rafiei (2015) considers the effect of xenon concentration. The sliding surface is designed as a difference between actual neutron density/reactor power and desired neutron density/reactor power. However, with the designed sliding surface, one cannot directly apply the second-order STA to the considered system to achieve finite-time stability as the relative degree of the system is two. Hui et al. (2020) proposed a high-gain observer based adaptive super-twisting sliding mode controller to control the power level of a modular high-temperature gas-cooled reactor. The high-gain observer is first constructed to estimate the unmeasured states of the system and then based on the estimated information an adaptive super-twisting sliding mode controller is designed. Abdurhaheem et al. (2021) proposed both twisting algorithm and STA based controllers to regulate the nuclear reactor power. The robustness of the twisting controller is shown in the presence of external disturbance and parameter variations through simulation results. The authors concluded that an STA-based controller could replace the twisting controller without compromising the performance indices.

In Surjagade et al. (2020), a chattering free optimal controller is proposed to regulate the total power of a pressurized heavy water reactor. To avoid chattering, the discontinuous control of an SMC is replaced by an STA-based controller. Even though the STA-based controllers (Qaiser et al., 2009; Ansarifar and Rafiei, 2015; Hui et al., 2020; Abdurhaheem et al., 2021; Surjagade et al., 2020) are proposed to solve the problem of nuclear reactor control and to overcome the chattering problem but, those controllers cannot be applied directly to the systems with a higher relative degree, as they are restricted to a relative degree one system. Thus, for higher-order systems Kamal et al. (2014) and Mishra et al. (2016) proposed arbitrary-order generalized STA-based controllers which produce a continuous control action and thereby avoid the chattering problem by preserving all the properties of a first-order SMC. Thus, makes it suitable for practical applications.

In this paper, an arbitrary order STA-based controller (n-STA) is proposed for a non-linear PWR-type NPP. The proposed controller produces a continuous control input. The proposed control scheme is easy to implement and requires only the information about system output and thus, it significantly reduces the complexity of the control architecture. The proposed controller is applied to control different subsystems of an NPP. Specifically, the control is designed and tested for reactor core power, steam generator pressure, pressurizer pressure and level, and turbine speed. Comparison with other classical control schemes such as Linear Quadratic Gaussian Integral Sliding Mode Control (LQG-ISMC) and Proportional-Integral (PI) controller is performed for different control loops of a PWR. The major contributions of the proposed work are summarized as follows:

1. The proposed controller guarantees finite time convergence to the desired set-point.
2. The proposed control algorithm uses only the output information to synthesize the controller.
3. Different control problems of nuclear power plant are considered such as reactor core power control, steam generator pressure control, pressurizer pressure and level control, and turbine speed control.

The rest of the paper is organized as follows: Section 2 formulates the control problem and explains the design procedure of the proposed controller. The brief introduction of non-linear dynamical model of PWR nuclear power plant is given in Section 3. The effectiveness of the proposed controller is demonstrated in Section 4 by performing simulation studies on PWR-type NPP. In Section 5 numerical analysis of the proposed controller is performed. Finally, conclusions are drawn in Section 6 indicating main contributions and scope for future work.

2. Design of generalized super-twisting algorithm based controller

2.1. Problem formulation

Let us consider an uncertain nonlinear dynamic single input system of the form

$$\dot{x}(t) = f(x(t), t) + b(x(t), t)u(t), \quad (1a)$$

$$y(t) = s(x(t), t), \quad (1b)$$

where $x(t) \in \mathbb{R}^n$ is the vector of system state variables, $u(t) \in \mathbb{R}$ is the control input, $y(t) \in \mathbb{R}$ is the system output, t is the independent time variable, $f(x(t), t) \in \mathbb{R}^n$ and $b(x(t), t) \neq 0 \in \mathbb{R}^n$ are the uncertain vector functions, $s(x(t), t)$ is the smooth measurable output function, which is also called as sliding variable. Here, the control objective is to design a robust nonlinear, high tracking precision, low chattering level SMC strategy for a nonlinear system (1).

2.2. Proposed approach

The controller design is initiated by defining the output tracking error $e(t)$ as

$$e(t) = y(t) - y_d(t), \quad (2)$$

where $y_d(t) \in \mathbb{R}$ is the desired output. The SMC is designed in two steps, in the first step, a stable sliding surface is designed, and in the second step, a control law is designed. In order to achieve finite time convergence and better tracking performance here, the proportional derivative (PD) nonsingular terminal sliding surface (Feng et al., 2002) is designed as follows

$$s(t) = K_P e(t) + K_D \dot{e}(t)^{(\kappa_1/\kappa_2)}, \quad (3)$$

where $K_P > 0$ and $K_D > 0$ are the proportional and derivative gains, respectively and κ_1 and κ_2 are positive odd integers which satisfy the following condition:

$$1 < \kappa_1/\kappa_2 < 2.$$

For system (1), the following assumptions are made:

1. The relative degree of the system (1) with respect to the sliding variable $s(x(t), t)$ is constant and known, and it is assumed to be equal to r .
2. An exact robust differentiator is available for exactly measuring or estimating the derivatives of variables.

Assumption 1 means that the control input $u(t)$ first appears explicitly only in the r th order total time derivative of sliding variable $s(x(t), t)$ and $\frac{d}{du} s^r(x(t), t) \neq 0$ at the given point. Considering the nonlinear system (1), and let the system be closed by some possibly dynamic discontinuous feedback control. Provided that, $s(x(t), t)$, $\dot{s}(x(t), t)$, ..., $s^{(r-1)}(x(t), t)$ are continuous function of t and $x(t)$, the corresponding motion will correspond to an r th order sliding or r -sliding mode and the set

$$\Sigma^r = \left\{ x(t) \mid s(x(t), t) = \dot{s}(x(t), t) = \dots = s^{(r-1)}(x(t), t) = 0 \right\} \quad (4)$$

called the r th order sliding set, is non-empty and is locally an integral set in the Filippov sense (Filippov, 1988). The higher order SMC approach allows the finite time stabilization to zero of $s(x(t), t)$, $\dot{s}(x(t), t)$, ..., $s^{(r-1)}(x(t), t)$ by defining a suitable discontinuous control function. Finding the r th order total time derivative of $s(x(t), t)$ along the trajectories of (1) gives

$$s^r(x(t), t) = \varphi(x(t), t) + \gamma(x(t), t)u(t), \quad (5)$$

where the uncertain functions

$$\varphi(x(t), t) = s^r(x(t), t)|_{u(t)=0}$$

and

$$\gamma(x(t), t) = \frac{\delta}{\delta u} s^r(x(t), t) \neq 0$$

are assumed to be bounded. Without loss of generality, one suppose that the uncertain vector functions $\varphi(x(t), t)$ and $\gamma(x(t), t)$ holds conditions

$$-\Phi \leq \varphi(x(t), t) \leq \Phi, \quad (6)$$

and

$$0 < \Gamma_m \leq \gamma(x(t), t) \leq \Gamma_M, \quad (7)$$

globally for some $\Phi, \Gamma_m, \Gamma_M \geq 0$, respectively. Note that at least locally (6) and (7) are satisfied for any smooth system (1) with well defined relative degree r . In the sequel, for simplicity, $\bullet(t)$ will be used for $\bullet(x(t), t)$ for all the variable \bullet .

Let us define the local coordinates

$$z(t) = \begin{bmatrix} z_1(t) \\ z_2(t) \\ \vdots \\ z_{(r-1)}(t) \\ z_r(t) \end{bmatrix} = \begin{bmatrix} s(t) \\ \dot{s}(t) \\ \vdots \\ s^{(r-2)}(t) \\ s^{(r-1)}(t) \end{bmatrix}$$

Then, (5) can be represented in terms of chain of integrators form as follows

$$\begin{aligned} \dot{z}_1(t) &= z_2(t) \\ \dot{z}_2(t) &= z_3(t) \\ &\vdots \\ \dot{z}_{(r-1)}(t) &= z_r(t) \\ \dot{z}_r(t) &= \varphi(t) + \gamma(t)u(t). \end{aligned} \quad (8)$$

System (8) can be rewritten as

$$\begin{aligned} \dot{z}_i(t) &= z_{i+1}(t) \\ \dot{z}_r(t) &= \underbrace{\varphi(t) + (\gamma(t) - 1)u(t)}_{\phi(t)} + u(t), \end{aligned} \quad (9)$$

for $1 \leq i \leq (r-1)$. It yields

$$\begin{aligned} \dot{z}_i(t) &= z_{i+1}(t) \\ \dot{z}_r(t) &= \phi(t) + u(t), \end{aligned} \quad (10)$$

where the lumped uncertainty $\phi(t)$ represents the uncertainties due to parameters variation, unmodelled dynamics and/or external disturbances. It is assumed that the uncertainty $\phi(t)$ is Lipschitz (in time) continuous uncertainty, which satisfies

$$|\dot{\phi}(t)| \leq \phi^*, \quad (11)$$

where ϕ^* is a known positive constant. Note that, practically (11) is feasible because almost all the physical systems have bounded states.

To achieve the control objective, an arbitrary order generalized STA based controller (n-STA) (Kamal et al., 2014) is employed for system (10) having relative degree r with respect to output. The generalized STA based controller (Kamal et al., 2014) is designed as

$$u(t) = -\mu_1 |\psi_{r-1}(t)|^{1/2} \text{sign}(\psi_{r-1}(t)) + u_r(t) \quad (12a)$$

$$\dot{u}_r(t) = -\mu_{r+1} \text{sign}(\psi_{r-1}(t)), \quad (12b)$$

where $\psi_{r-1}(t)$ can be obtained in three steps as follows:

1. Defining

$$K_{1,r-1} = |z_1(t)|^{\frac{r}{r+1}}$$

where r represents the relative degree of system with respect to $z_1(t)$. For all $i = 2, 3, \dots, (r-1)$, the $K_{i,r-1}$ is defined as follows

$$K_{i,r-1} = \left| |z_1(t)|^{p_1} + |z_2(t)|^{p_2} + \dots + |z_{i-2}(t)|^{p_{i-2}} \right|^{q_i}$$

where p_1, p_2, \dots, p_{i-2} and q_i are designed based on the homogeneity weight of the $z_{i+1}(t)$.

2. Again defining

$$L_{0,r-1} = z_1(t)$$

$$L_{1,r-1} = z_2(t) + \mu_2 K_{1,r-1} \text{sign}(z_1(t))$$

and for all $i = 2, 3, \dots, (r-1)$, the $L_{i,r-1}$ is defined as follows

$$L_{i,r-1} = z_{i+1}(t) + \mu_{i+1} K_{i,r-1} \text{sign}(L_{i-1,r-1}). \quad (13)$$

3. Finally

$$\psi_{r-1}(t) = L_{r-1,r-1}. \quad (14)$$

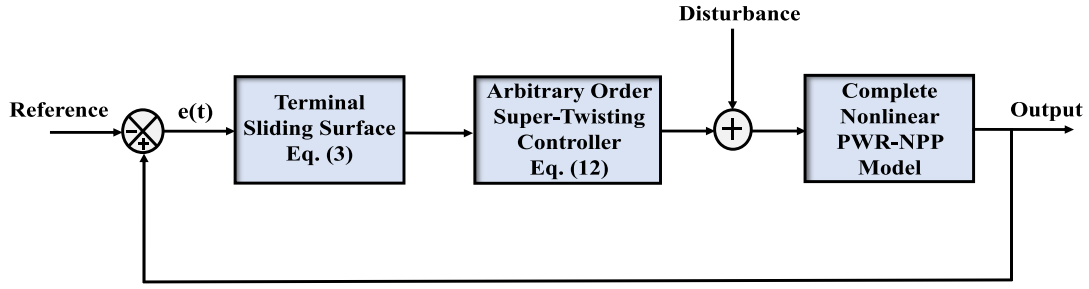


Fig. 1. Schematic of overall control scheme.

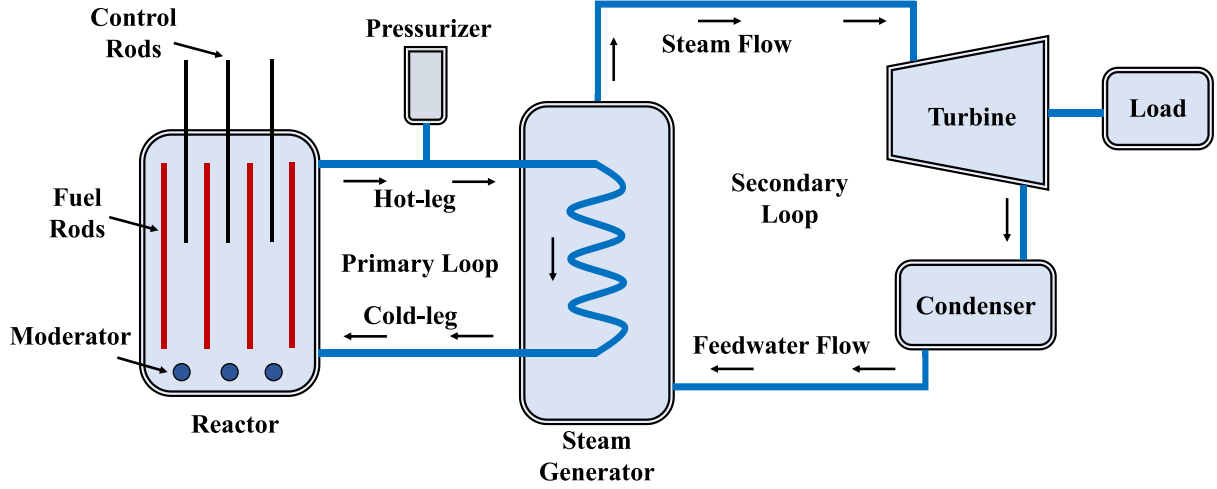


Fig. 2. A simple block diagram representation of different interconnected subsystems in a PWR nuclear power plant.

For stability proof and selection of gains of STA based controllers, readers are kindly referred to [Kamal et al. \(2014\)](#), [Moreno and Osorio \(2012\)](#), [Surjagade et al. \(2020\)](#) and [Mishra et al. \(2016\)](#).

The block diagram of the proposed control scheme is shown in [Fig. 1](#).

3. Dynamic model of PWR nuclear power plant

In this work, the nonlinear dynamic model of PWR type nuclear reactor and its associated subsystems given in Ref. [Vajpayee et al. \(2020b\)](#) and [Vajpayee et al. \(2021b\)](#) is adopted for the study. The model considers the dynamics of the reactor core, thermal hydraulics, piping and plenum, pressurizer, steam generator, condenser, and turbine-governor system, in addition to various actuators and sensors. A simplified block diagram of the PWR-type nuclear power plant showing interconnections of various systems is shown in [Fig. 2](#). A detailed description of derivation of model equations of different systems, definitions of variables and values of parameters used in this work can be found in [Vajpayee et al. \(2020b, 2021b\)](#). However, for brevity the dynamic equations of different systems are given below:

3.1. Normalized point kinetic reactor core model

$$\frac{dP_n}{dt} = \frac{\rho_t - \sum_{i=1}^6 \beta_i}{\Lambda} P_n + \sum_{i=1}^6 \frac{\beta_i}{\Lambda} C_{in}$$

$$\frac{dC_{in}}{dt} = \lambda_i P_n - \lambda_i C_{in}, \quad i = 1, 2, \dots, 6$$

3.2. Thermal hydraulics model

$$\frac{dT_f}{dt} = H_f P_n - \frac{1}{\tau_f} (T_f - T_{c1})$$

$$\frac{dT_{c1}}{dt} = H_c P_n + \frac{1}{\tau_c} (T_f - T_{c1}) - \frac{2}{\tau_r} (T_{c1} - T_{rxi})$$

$$\frac{dT_{c2}}{dt} = H_c P_n + \frac{1}{\tau_c} (T_f - T_{c1}) - \frac{2}{\tau_r} (T_{c2} - T_{c1})$$

3.3. Piping and plenum model

$$\frac{dT_{rxu}}{dt} = \frac{1}{\tau_{rxu}} (T_{c2} - T_{rxu})$$

$$\frac{dT_{hot}}{dt} = \frac{1}{\tau_{hot}} (T_{rxu} - T_{hot})$$

$$\frac{dT_{sgl}}{dt} = \frac{1}{\tau_{sgl}} (T_{hot} - T_{sgl})$$

$$\frac{dT_{sgu}}{dt} = \frac{1}{\tau_{sgu}} (T_{p2} - T_{sgu})$$

$$\frac{dT_{cold}}{dt} = \frac{1}{\tau_{cold}} (T_{sgu} - T_{cold})$$

$$\frac{dT_{rxi}}{dt} = \frac{1}{\tau_{rxi}} (T_{cold} - T_{rxi})$$

3.4. Steam generator model

$$\frac{dT_{p1}}{dt} = \frac{1}{\tau_{p1}} (T_{sgl} - T_{p1}) - \frac{1}{\tau_{pm1}} (T_{p1} - T_{m1})$$

$$\begin{aligned}\frac{dT_{p2}}{dt} &= \frac{1}{\tau_{p2}} (T_{p1} - T_{p2}) - \frac{1}{\tau_{pm2}} (T_{p2} - T_{m2}) \\ \frac{dT_{m1}}{dt} &= \frac{1}{\tau_{mp1}} (T_{p1} - T_{m1}) - \frac{1}{\tau_{ms1}} (T_{m1} - T_s) \\ \frac{dT_{m2}}{dt} &= \frac{1}{\tau_{mp2}} (T_{p2} - T_{m2}) - \frac{1}{\tau_{ms2}} (T_{m2} - T_s) \\ \frac{dp_s}{dt} &= \frac{1}{K_s} \left[U_{ms1} S_{ms1} (T_{m1} - T_s) + U_{ms2} S_{ms2} (T_{m2} - T_s) \right. \\ &\quad \left. - \dot{m}_{so} (h_{ss} - c_{pfw} T_{fw}) \right] \\ K_s &= m_{ws} \frac{\partial h_{ws}}{\partial p_s} + m_{ss} \frac{\partial h_{ss}}{\partial p_s} - m_{ws} \left(\frac{h_{ws} - h_{ss}}{v_{ws} - v_{ss}} \right) \frac{\partial v_{ss}}{\partial p_s} \\ \dot{m}_{so} &= C_{ig} p_s \\ T_s &= \frac{\partial T_{sat}}{\partial p_s} p_s\end{aligned}$$

3.5. Pressurizer model

$$\begin{aligned}\frac{dl_w}{dt} &= \frac{1}{d_s A_p} \left[\left(A_p (l - l_w) K_{2p} - \frac{C_{2p}}{C_{1p}} \right) \frac{dp_p}{dt} \right. \\ &\quad \left. + \frac{1}{C_{p1}^2} \left(C_{2p} \frac{dp_p}{dt} - \dot{m}_{sur} - \dot{m}_{spr} \right) + \frac{\dot{m}_{sur}}{C_{1p}} \right] \\ \frac{dp_p}{dt} &= \frac{Q_{heat} + \dot{m}_{sur} \left(\frac{p_p v_s}{J_p C_{1p}} + \frac{h_{\bar{w}}}{C_{1p}} \right) + \dot{m}_{spr} \left(h_{spr} - h_w + \frac{h_{\bar{w}}}{C_{1p}} + \frac{p_p v_w}{J_p C_{1p}} \right)}{m_w \left(K_{3p} + \frac{K_{4p} p_p}{J_p} \right) + \frac{m_s K_{4p} p_p}{J_p} - \frac{V_w}{J_p} + \frac{C_{2p}}{C_{1p}} \left(h_{\bar{w}} + \frac{p_p v_s}{J_p} \right)} \\ \dot{m}_{sur} &= \sum_{j=1}^N V_j \theta_j \frac{dT_j}{dt} \\ C_{1p} &= \frac{d_w}{d_s} - 1 \\ C_{2p} &= A_p (l - l_w) \frac{d_w}{d_s} K_{2p} + A_p l_w K_{1p} \\ K_{1p} &= \frac{\partial d_w}{\partial p_p} \\ K_{2p} &= \frac{\partial d_s}{\partial p_p} \\ K_{3p} &= \frac{\partial h_w}{\partial p_p} \\ K_{4p} &= \frac{\partial v_s}{\partial p_p}\end{aligned}$$

3.6. Turbine model

$$\begin{aligned}\frac{d^2 P_{hp}}{dt^2} &+ \left(\frac{O_{rv} + \tau_{ip}}{\tau_{hp} \tau_{ip}} \right) \frac{dP_{hp}}{dt} + \left(\frac{O_{rv}}{\tau_{hp} \tau_{ip}} \right) P_{hp} \\ &= \left(\frac{O_{rv} F_{hp}}{\tau_{hp} \tau_{ip}} \right) \bar{m}_{so} + \left(\frac{(1 + \kappa_{hp}) F_{hp}}{\tau_{hp}} \right) \frac{d\bar{m}_{so}}{dt} \\ \frac{d^2 P_{ip}}{dt^2} &+ \left(\frac{O_{rv} \tau_{hp} + \tau_{ip}}{\tau_{hp} \tau_{ip}} \right) \frac{dP_{ip}}{dt} + \left(\frac{O_{rv}}{\tau_{hp} \tau_{ip}} \right) P_{ip} = \left(\frac{O_{rv} F_{ip}}{\tau_{hp} \tau_{ip}} \right) \bar{m}_{so} \\ \frac{d^3 P_{lp}}{dt^3} &+ \left(\frac{O_{rv} \tau_{hp} + \tau_{ip}}{\tau_{hp} \tau_{ip}} + \frac{1}{\tau_{lp}} \right) \frac{d^2 P_{lp}}{dt^2} \\ &+ \left(\frac{O_{rv} (\tau_{lp} + \tau_{hp}) + \tau_{ip}}{\tau_{hp} \tau_{ip} \tau_{lp}} \right) \frac{dP_{lp}}{dt} + \left(\frac{O_{rv}}{\tau_{hp} \tau_{ip} \tau_{lp}} \right) P_{lp} \\ &= O_{rv} F_{lp} \bar{m}_{so}\end{aligned}$$

$$\begin{aligned}\bar{m}_{so} &= \dot{m}_{so} / \dot{m}_{sor} \\ P_{tur} &= P_{hp} + P_{ip} + P_{lp} \\ \frac{d\omega_{tur}}{dt} &= \frac{P_{tur} - P_{dem}}{(2\pi)^2 J_{tur} \omega_{tur} I_{ig}}\end{aligned}$$

3.7. Condenser model

$$\begin{aligned}\frac{dh_{wo}}{dt} &= \frac{(\dot{m}_{coh} + \dot{m}_{cow}) (h_{cow} - h_{wo})}{m_{coh}} \\ \dot{m}_{coh} &= \dot{m}_{lp} - \dot{m}_{cow} \\ \dot{m}_{cow} &= \dot{m}_{lp} \frac{(h_{lp} - h_{cow})}{h_{c\bar{w}}} \\ \frac{d\dot{m}_{cos}}{dt} &= \frac{\dot{m}_{cow} - \dot{m}_{cos}}{\tau_{co}}\end{aligned}$$

3.8. Reactivity model

$$\begin{aligned}\rho_t &= \rho_{rod} + \rho_f + \rho_{c1} + \rho_{c2} + \rho_p \\ \rho_t &= \rho_{rod} + \alpha_f T_f + \alpha_c T_{c1} + \alpha_c T_{c2} + \alpha_p p_p\end{aligned}$$

3.9. Sensors

3.9.1. Ex-core detectors and amplifiers

$$\begin{aligned}\tau_1 \tau_2 \frac{d^2 i_{lo}}{dt^2} + (\tau_1 + \tau_2) \frac{di_{lo}}{dt} + i_{lo} &= K_{lo} \log_{10} (\kappa_{lo} P_n) \\ \tau_3 \tau_4 \frac{d^2 i_{lr}}{dt^2} + (\tau_3 + \tau_4) \frac{di_{lr}}{dt} + i_{lr} - 12 &= K_{lr} \frac{di_{lo}}{dt}\end{aligned}$$

3.9.2. Resistance temperature detector

$$\begin{aligned}\frac{dT_{rtd1}}{dt} &= \frac{1}{\tau_{rtd}} (-T_{rtd1} + 2T_{c1} - T_{rx1}) \\ \frac{dT_{rtd2}}{dt} &= \frac{1}{\tau_{rtd}} (-T_{rtd2} + 2T_{c2} - T_{rx2}) \\ i_{rtd} &= K_{rtd} \frac{(T_{rtd} - T_{rx10})}{(T_{rxu0} - T_{rx10})} + 4 \text{ mA} \\ T_{rtd} &= \frac{(T_{rtd1} + T_{rtd2})}{2}\end{aligned}$$

3.10. Actuators

3.10.1. Control rod

$$\frac{d\rho_{rod}}{dt} = G v_{rod}$$

3.10.2. Turbine-governor valve

$$\frac{d^2 C_{ig}}{dt^2} + 2\zeta_{ig} \omega_{ig} \frac{dC_{ig}}{dt} + \omega_{ig}^2 C_{ig} = \omega_{ig}^2 K_{ig} u_{ig}$$

3.10.3. Pressurizer heater

$$C_{heat} \frac{dQ_{heat}}{dt} + \frac{Q_{heat}}{R_{heat}} = K_{heat} i_{heat}$$

4. Simulation results and discussion

The proposed control algorithm is applied to the different control loops *i.e.*, reactor core power control loop, steam generator pressure control loop, pressurizer pressure and level control loop, and turbine speed control loop of PWR-type NPP and its performance is tested in the presence of external disturbance for set-point change. For the input–output information of each control loop, readers are kindly referred to Vajpayee et al. (2020b). In this simulation study, in each control loop a sinusoidal external disturbance in the control input is considered throughout system response as

$$\text{Disturbance} = d_0 \sin(0.1t), \quad (15)$$

where d_0 is the magnitude of the disturbance. To show the superiority of the proposed controller over some other control strategies, we have compared the results of the proposed nonlinear n-STA based controller with some existing conventional control strategies proposed in literature such as Linear Quadratic Gaussian Integral Sliding Mode Control (LQG-ISMC) proposed in Vajpayee et al. (2021a) and Proportional–Integral (PI) controller proposed in Vajpayee et al. (2020b).

The control expression for LQG-ISMC and PI controller is as follows (Vajpayee et al., 2020b, 2021a):

1. Linear Quadratic Gaussian Integral Sliding Mode Control (LQG-ISMC):

The total control $u(t)$ is designed as

$$u(t) = u_n(t) + u_d(t),$$

where $u_n(t)$ is the nominal control and $u_d(t)$ is the discontinuous control. The nominal control $u_n(t)$ is designed as

$$u_n(t) = -K_c \hat{x}(t) + R^{-1} B^T g(t),$$

where K_c is the Kalman gain, R is the positive definite weighing matrix, B is the input distribution matrix, $\hat{x}(t)$ is the estimated state vector and it is estimated by Kalman filter estimation problem, and $g(t)$ is the auxiliary variable which is a solution of

$$-\dot{g}(t) = (A - BK_c)^T g(t) + C^T Q y_d(t), \quad g(\infty) = 0.$$

In the above A is the state matrix, C is the output matrix, Q is the positive semidefinite weighing matrix, and $y_d(t)$ is the desired output. The discontinuous signal $u_d(t)$ is designed as

$$u_d(t) = \mu_d \frac{\sigma(t)}{\sigma(t) + \epsilon},$$

where $\mu_d > 0$ is the discontinuous gain, ϵ is the small positive constant, and $\sigma(t)$ is the sliding surface and it is designed as

$$\sigma(t) = (B^T B)^{-1} B^T \left[\hat{x}(t) - \hat{x}(0) - \int_0^t \hat{\dot{x}}_n(\tau) d\tau \right].$$

2. Proportional–Integral (PI) controller:

The control signal for PI controller is designed as

$$u(t) = \left(K_1 + \frac{K_2}{s} \right) (y_d(t) - y(t)),$$

where K_1 is the proportional gain, K_2 is the integral gain, $y(t)$ is the system output, and $y_d(t)$ is the desired output.

The values of tuned control gains of LQG-ISMC and PI controller are given in Table 1.

4.1. Reactor power control loop

4.1.1. Load following mode of operation

In the load-following mode of operation, the reactor power adjusts according to electricity demand throughout the day. In this control loop, objective is to track the demand power variation precisely in

Table 1

Control gains for LQG-ISMC and PI controller.

Control loop	LQG-ISMC					PI	
	Q	R	Ξ	Θ	μ_d	K_1	K_2
Reactor power	$1 \times 10^{-3} I_n$	1×10^5	$5 I_n$	1	1	3.1×10^{-2}	4×10^{-3}
SG pressure	$5 \times 10^{-3} I_n$	1×10^2	$5 \times 10^{-5} I_n$	1	0.1	4.7×10^{-1}	1×10^{-1}
Heater	$1 I_n$	1×10^{-8}	$1 \times 10^{-2} I_n$	1	25	1.1×10^7	6.4×10^6
Spray	$5 \times 10^{-3} I_n$	1×10^{-8}	$5 \times 10^{-5} I_n$	1	0.2	3×10^5	1.7×10^5
Pressurizer level	$1 \times 10^3 I_n$	1×10^{-2}	$6 I_n$	1	0.1	1.3×10^3	7.4×10^2
Turbine speed	$2 \times 10^3 I_n$	1×10^{-2}	$1 I_n$	1	0.1	1.5×10^3	5.4×10^{-1}

spite of presence of uncertainties in the system. The reactor power is controlled by varying the control rod movement speed, $v_{rod}(t)$ and the reactor power is measured with the help of excore detector current, $i_{lo}(t)$. With this input–output combination, the relative degree of the system (corresponds to this control loop) with respect to output is 3. Thus, for this control loop 4-STA based controller is proposed as follows

$$u(t) = -\mu_1 |\psi_2(t)|^{1/2} \text{sign}(\psi_2(t)) + u_3(t), \quad (16a)$$

$$\dot{u}_3(t) = -\mu_4 \text{sign}(\psi_2(t)), \quad (16b)$$

where

$$\psi_2(t) = z_3(t) + \mu_3 \left[|z_1(t)|^3 + |z_2(t)|^4 \right]^{1/6} \times \text{sign}(z_2(t) + \mu_2 |z_1(t)|^{3/4} \text{sign}(z_1(t))).$$

In (16), the values of μ_1 , μ_2 , μ_3 and μ_4 are selected as 1×10^{-4} , 1×10^{-2} , 1×10^{-2} and 1×10^{-2} , respectively. To design a sliding surface an error signal is defined as

$$e(t) = i_{lo}(t) - i_{lo}^{ref}(t)$$

and the values of K_p , K_D , κ_1 , and κ_2 in (3) are selected as 1, 1, 11, and 9, respectively. The reference excore detector current corresponds to demand power is varied as follows:

$$i_{lo}^{ref} = \begin{cases} 19.6554, & 0 \leq t \leq 200 \\ -9.485 \times 10^{-3}(t - 200) + 19.6554, & 200 < t \leq 220 \\ 19.4657, & 220 < t \leq 1000 \\ 1.001 \times 10^{-3}(t - 1000) + 19.4657, & 1000 < t \leq 1100 \\ 19.5658, & 1100 < t \leq 1500 \\ 8.9600 \times 10^{-4}(t - 1500) + 19.5658, & 1500 < t \leq 1600 \\ 19.6554 & \text{elsewhere.} \end{cases}$$

To show the robustness of the proposed controller in the presence of external disturbance, an inadvertent sinusoidal perturbation is considered throughout the system response in $v_{rod}(t)$ as in (15) where the value of d_0 is selected as 1×10^{-4} . During the transient, variation of excore detector logarithmic amplifier output current, $i_{lo}(t)$ correspond to the reactor power with the proposed controller, the LQG-ISMC and the PI controller is shown in Fig. 3. It can be observed that the proposed controller and the LQG-ISMC are able to follow the change in demand despite the presence of disturbance in the system but, the performance of the closed-loop system is improved much with the proposed nonlinear controller as compared to the linear LQG-ISMC, as evident from the deviation of system output from the desired output, shown in Fig. 4. Whereas, the PI controller fails to maintain the system output closed to demand. Variation of reactor power and control input for three controllers are shown in Figs. 5 and 6, respectively. Variation of sliding surface for the proposed controller is shown in Fig. 7.

4.1.2. Sudden load decrement in emergency situation

In this simulation study, another transient is considered to validate the performance of the proposed controller during a sudden load decrement in emergency situation. The controller is designed in a similar

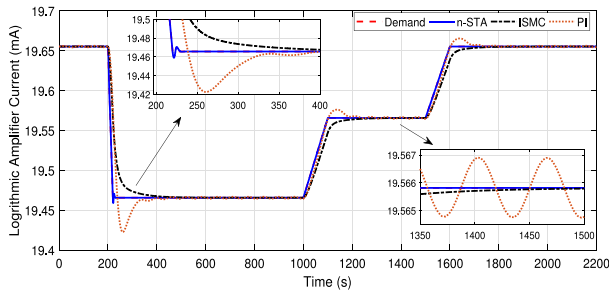


Fig. 3. Excore detector current during demand power manoeuvring.

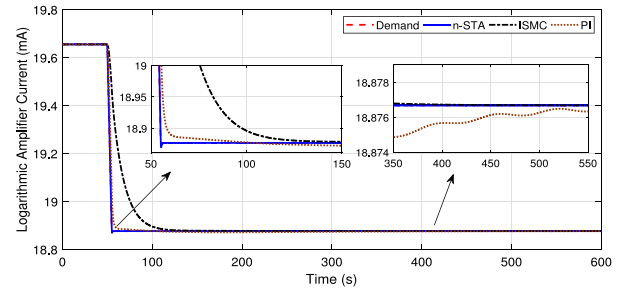


Fig. 8. Excore detector current during demand power manoeuvring.

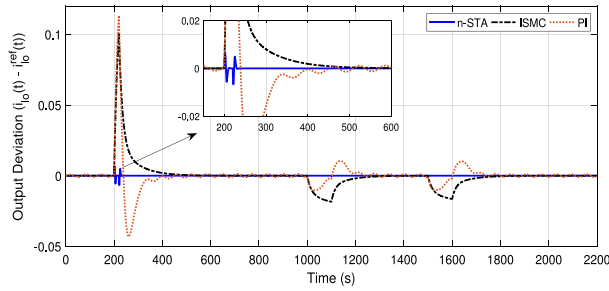


Fig. 4. Difference between reference signal and output signal during transient.

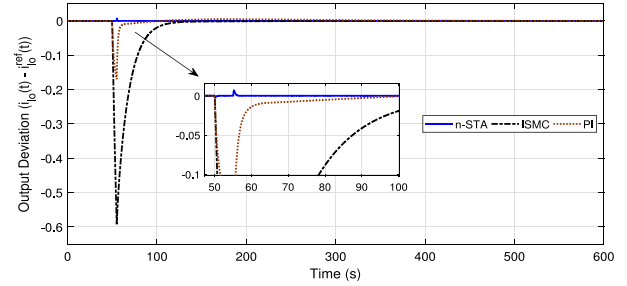


Fig. 9. Difference between reference signal and output signal during transient.

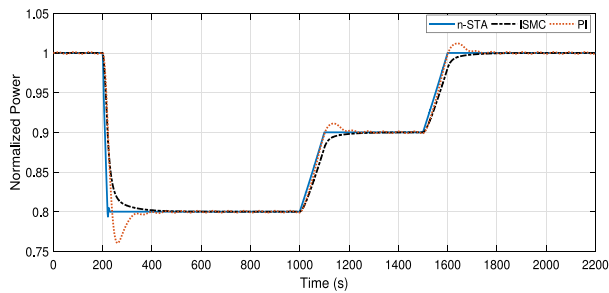


Fig. 5. Normalized reactor power during transient.

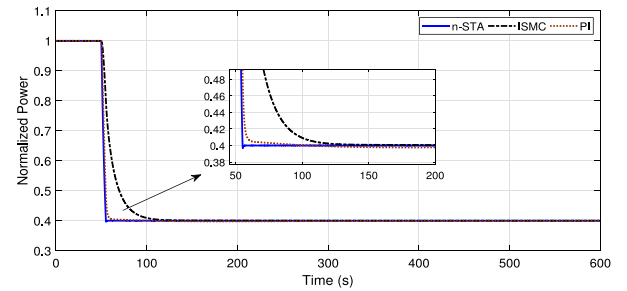


Fig. 10. Normalized reactor power during transient.

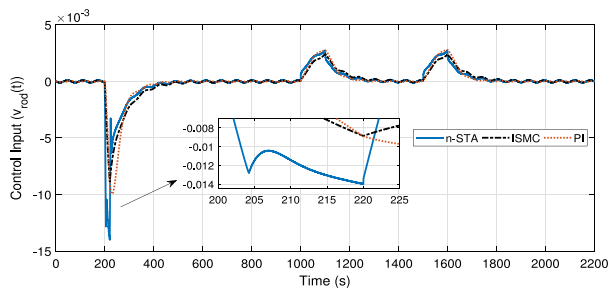


Fig. 6. Control rod speed moment during demand power manoeuvring.

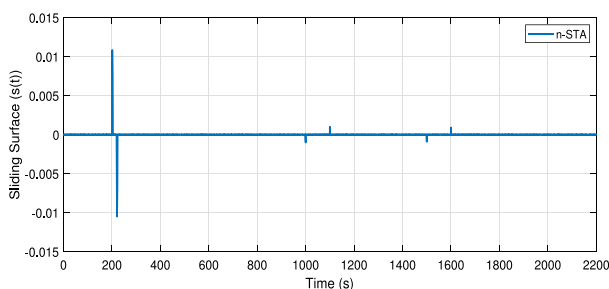


Fig. 7. Variation of sliding surface during demand power manoeuvring.

way as designed in Section 4.1.1. To show the effectiveness of the proposed controller in case of large demand power variations from steady state, the demand power is brought down from full power to 40% of full power in 5 s. During the transient, variation of excore detector logarithmic amplifier output current, $i_{lo}(t)$ correspond to the reactor power with the proposed controller, the LQG-ISMC and the PI controller is shown in Fig. 8. In this case also, it can be observed that the performance of the closed-loop system is improved with the proposed controller as compared to the LQG-ISMC and PI controller, as evident from the deviation of system output from the desired output, shown in Fig. 9. Variation of reactor power and control input for three controllers are shown in Figs. 10 and 11, respectively. Variation of sliding surface for the proposed controller is shown in Fig. 12.

4.2. Steam generator pressure control loop

In this control loop, objective is to maintain the pressure in steam generator. The steam generator pressure, $P_s(t)$ is controlled by adjusting the input signal to the turbine-governor valve, $u_{tg}(t)$. With this input-output combination, the relative degree of the system with respect to output is 2. Thus, for this control loop 3-STA based controller is proposed as follows

$$u(t) = -\mu_1 |\psi_1(t)|^{1/2} \text{sign}(\psi_1(t)) + u_2(t), \quad (17a)$$

$$\dot{u}_2(t) = -\mu_3 \text{sign}(\psi_1(t)), \quad (17b)$$

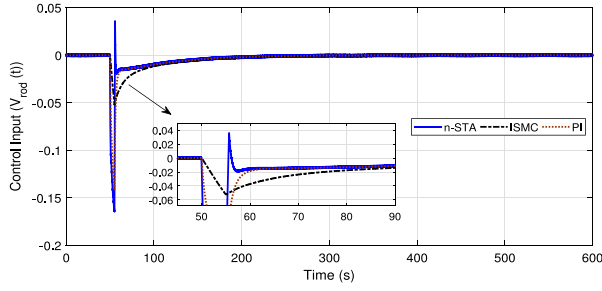


Fig. 11. Control rod speed moment during demand power manoeuvring.

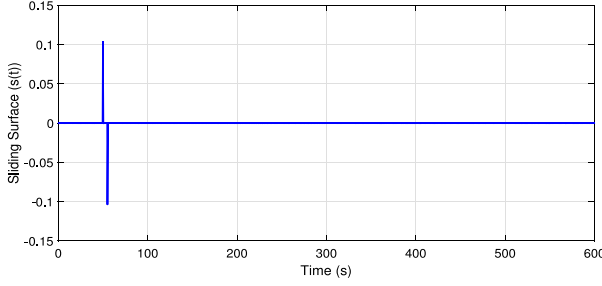


Fig. 12. Variation of sliding surface during demand power manoeuvring.

where

$$\psi_1(t) = z_2(t) + \mu_2 |z_1(t)|^{2/3} \text{sign}(z_1(t)).$$

In (17), the values of μ_1 , μ_2 and μ_3 are selected as 5×10^{-1} , 1×10^{-2} and 1×10^{-2} , respectively. To design a sliding surface an error signal is defined as

$$e(t) = P_s(t) - P_s^{ref}(t),$$

and the values of K_P , K_D , κ_1 , and κ_2 in (3) are selected as 4, 4, 11, and 9, respectively. The reference signal change in secondary pressure is applied as follows:

$$P_s^{ref} = \begin{cases} 7.2857, & 0 \leq t \leq 200 \\ 2.215 \times 10^{-4}(t - 200) + 7.2857, & 200 < t \leq 400 \\ 7.3300, & 400 < t \leq 1000 \\ -2.215 \times 10^{-4}(t - 1000) + 7.3300, & 1000 < t \leq 1200 \\ 7.2857, & \text{elsewhere.} \end{cases}$$

The performance of the proposed controller is evaluated in the presence of sinusoidal external disturbance for the above set-point change in steam generator secondary pressure. The sinusoidal disturbance in the control input, $u_{ig}(t)$ is considered throughout the system response as in (15) where the value of d_0 is selected as 1×10^{-3} . During the transient, variation of output secondary pressure with the proposed controller, the LQG-ISMC and the PI controller is shown in Fig. 13. Deviation of output pressure from desired pressure is shown in Fig. 14. It can be observed that the proposed controller is able to follow the set-point change more precisely compared to the LQG-ISMC and the PI controller. Fig. 15 shows the variation of input signal to turbine-governor valve. Variation of sliding surface for the proposed controller is shown in Fig. 16.

4.3. Pressurizer control loop

In this control loop, aim is to maintain the coolant pressure within a permissible limit. Primary coolant pressure can be controlled by a

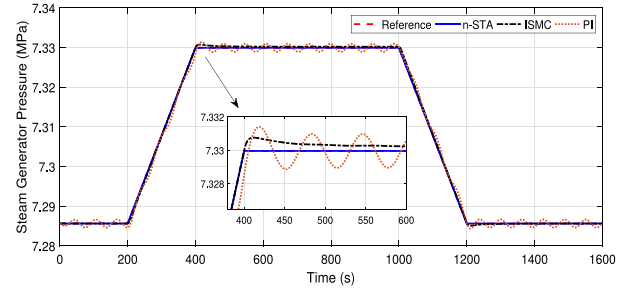


Fig. 13. Steam generator secondary pressure during set-point change.

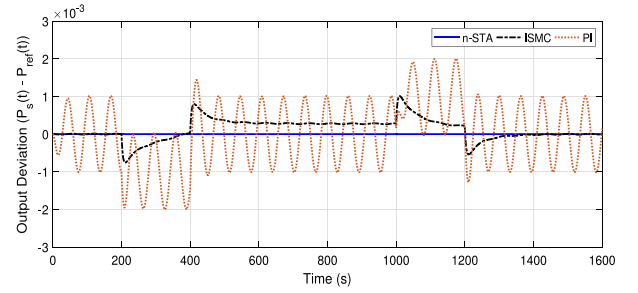


Fig. 14. Difference between reference signal and output signal during transient.

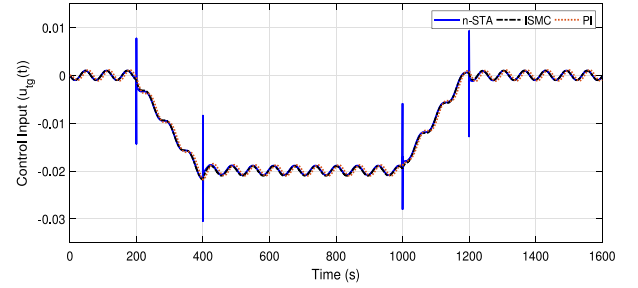


Fig. 15. Control signal to turbine-governor valve.

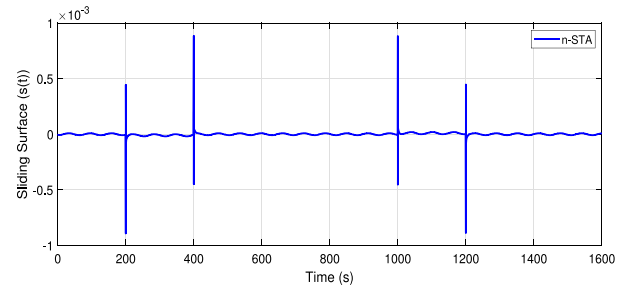


Fig. 16. Variation of sliding surface during set-point change.

bank of heaters, spray flow rate, power-operated relief valves, or safety valves. However, in this study, the coolant pressure is controlled by actuating a bank of heaters and by varying the spray flow rate.

4.3.1. Pressurizer pressure control by heater

For this control loop, the control input to the system is the rate of heat added by the heater, $Q_{heat}(t)$ and the output from the system is pressurizer pressure, $P_p(t)$. With this input-output combination, the relative degree of the system with respect to output is 1. Thus, for this control loop 2-STA based controller is proposed as follows

$$u(t) = -\mu_1 |\psi_0(t)|^{1/2} \text{sign}(\psi_0(t)) + u_1(t), \quad (18a)$$

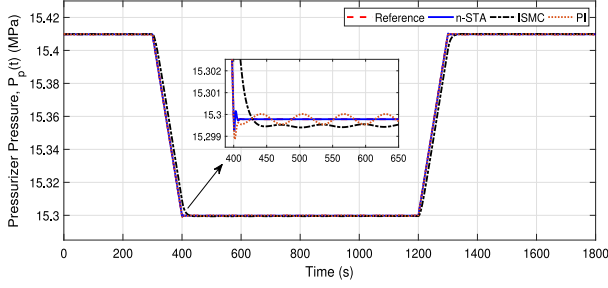


Fig. 17. Pressurizer pressure controlled by heater.

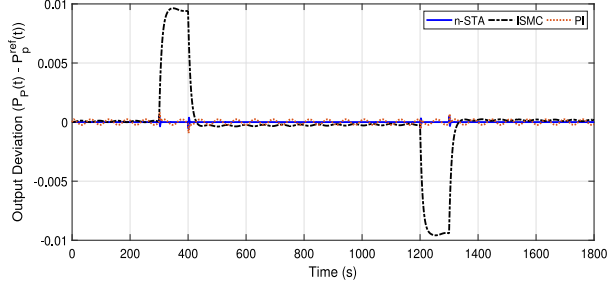


Fig. 18. Difference between reference signal and output signal during transient.

$$\dot{u}_1(t) = -\mu_2 \text{sign}(\psi_0(t)), \quad (18b)$$

where

$$\psi_0(t) = z_1(t).$$

In (18), the values of μ_1 and μ_2 are selected as 5×10^2 and 1.5×10^4 , respectively. To design a sliding surface an error signal is defined as

$$e(t) = P_p(t) - P_p^{ref}(t),$$

and the values of K_p , K_D , κ_1 , and κ_2 in (3) are selected as 1, 1.2, 11 and 9, respectively. The reference pressurizer pressure is varied as follows:

$$P_p^{ref} = \begin{cases} 15.4098, & 0 \leq t \leq 300 \\ -1.1 \times 10^{-3}(t - 300) + 15.4098, & 300 < t \leq 400 \\ 15.3000, & 400 < t \leq 1200 \\ 1.1 \times 10^{-3}(t - 1200) + 15.3000, & 1200 < t \leq 1300 \\ 15.4098, & \text{elsewhere.} \end{cases}$$

The performance of the proposed controller is tested for the above set-point change in the pressurizer pressure in the presence of sinusoidal external disturbance. The sinusoidal disturbance in the control input, $Q_{heat}(t)$ is considered from the beginning of the simulation as in (15) where the value of d_0 is considered as 1×10^4 . During this transient, variation of pressurizer pressure with the proposed controller, the LQG-ISMC and the PI controller is shown in Fig. 17. Deviation of output pressurizer pressure from the reference pressure is shown in Fig. 18. It can be observed that the proposed controller is able to follow the reference signal more precisely compared to the LQG-ISMC and the PI controller. Fig. 19 shows the variation of control input. The sliding surface plot for the proposed controller is shown in Fig. 20.

4.3.2. Pressurizer pressure control by spray

For this control loop, the control input to the system is mass spray flow rate, $\dot{m}_{spr}(t)$ and the system output is pressurizer pressure, $P_p(t)$. With this input-output combination, the relative degree of the system with respect to output is 1. Thus, similar to controller proposed in (18)

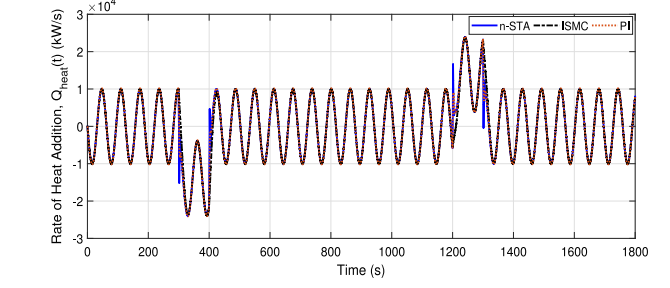


Fig. 19. Variation of rate of heat addition.

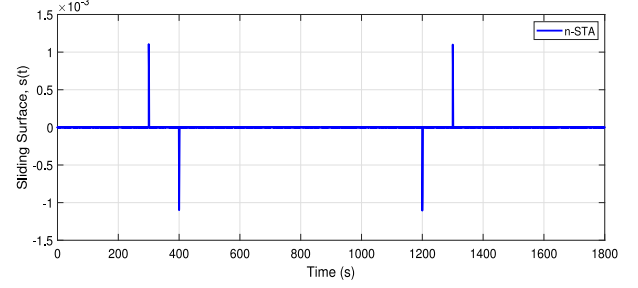


Fig. 20. Variation of sliding surface during set-point change.

in Section 4.3.1, for this control loop also 2-STA based controller is designed. Here, the values of μ_1 and μ_2 are selected as 1.5×10^2 and 1×10^3 , respectively. To design a sliding surface an error signal is also defined similar to one defined in Section 4.3.1 and the values of K_p , K_D , κ_1 , and κ_2 in (3) are selected as 1, 1, 11, and 9, respectively. In this study, the reference pressurizer pressure is varied as follows

$$P_p^{ref} = \begin{cases} 15.4098, & 0 \leq t \leq 200 \\ 1 \times 10^{-3}(t - 200) + 15.4098, & 200 < t \leq 220 \\ 15.43, & \text{elsewhere.} \end{cases}$$

Similar to the study conducted in Section 4.3.1, here also controller performance for a set-point change in pressurizer pressure is evaluated in the presence of sinusoidal external disturbance. The disturbance in the control input, $\dot{m}_{spr}(t)$ is considered throughout the system response as in (15) and the value of d_0 is considered as 1×10^2 . Fig. 21 shows the variation of output pressurizer pressure with respect to the reference signal for the proposed controller, the LQG-ISMC, and the PI controller. Deviation of output pressure from reference pressure for three controllers is shown in Fig. 22. In this case also the performance of the proposed controller is superior to the LQG-ISMC and the PI controller. Variation of control input is shown in Fig. 23. Fig. 24 shows the plot for the sliding surface for the proposed controller.

4.4. Pressurizer level control loop

The purpose of the pressurizer level control loop is to maintain the water level for the reactor core coolant system. For this control loop, the control input to the system is mass surge flow rate, $\dot{m}_{sur}(t)$ and the output from the system is pressurizer level, $l_w(t)$. With this input-output combination, the relative degree of the system with respect to output is 1. Thus, similar to controller proposed in (18) in Section 4.3.1, for this control loop also 2-STA based controller is designed. Here, the values of μ_1 and μ_2 are selected as 5 and 20, respectively. To design a sliding surface an error signal is defined as

$$e(t) = l_w(t) - l_w^{ref}(t),$$

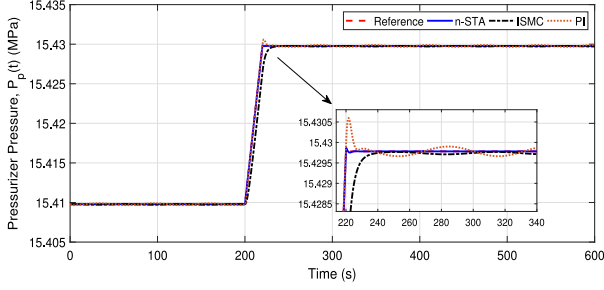


Fig. 21. Pressurizer pressure controlled by spray.

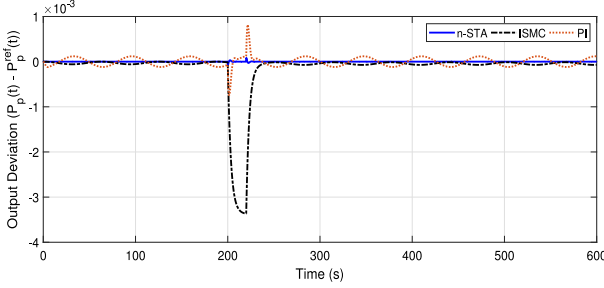


Fig. 22. Difference between reference signal and output signal during transient.

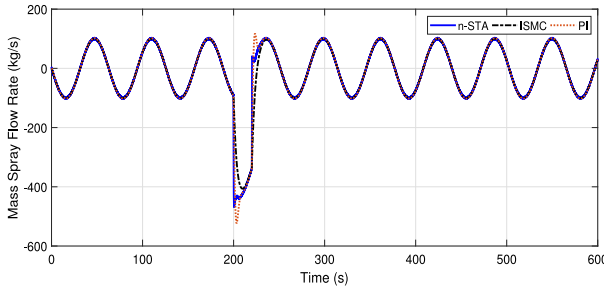


Fig. 23. Variation of rate of spray flow.

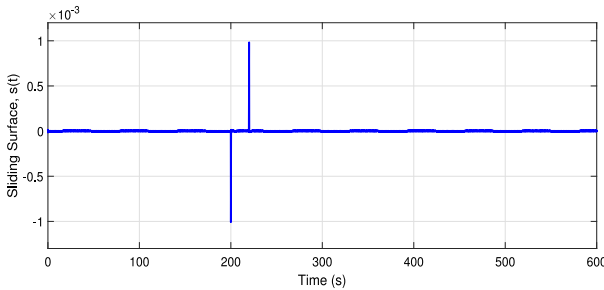


Fig. 24. Variation of sliding surface during set-point change.

and the values of K_p , K_D , κ_1 , and κ_2 in (3) are selected as 1, 1, 11, and

9, respectively. The reference pressurizer water level is varied in the

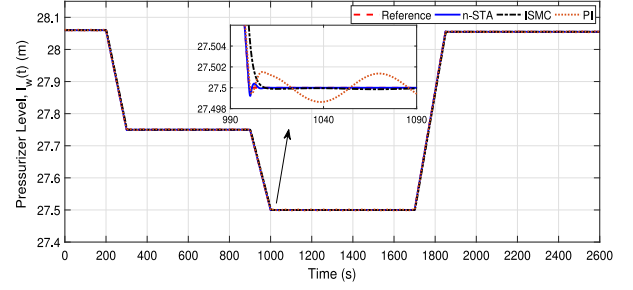


Fig. 25. Pressurizer level during transient.

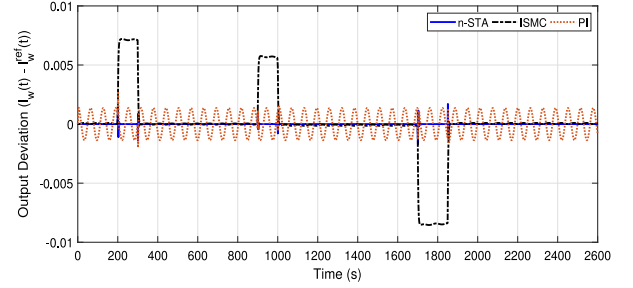


Fig. 26. Difference between reference pressurizer level and output level during transient.

following manner:

$$l_w^{ref} = \begin{cases} 28.06, & 0 \leq t \leq 200 \\ -3.1 \times 10^{-3}(t - 200) + 28.06, & 200 < t \leq 300 \\ 27.75, & 300 < t \leq 900 \\ -2.5 \times 10^{-3}(t - 900) + 27.75, & 900 < t \leq 1000 \\ 27.50, & 1000 < t \leq 1700 \\ 3.7 \times 10^{-3}(t - 1700) + 27.50, & 1700 < t \leq 1850 \\ 28.06, & \text{elsewhere.} \end{cases}$$

The robustness of the proposed controller is analysed in the presence of sinusoidal external disturbance for the above set-point variation in the pressurizer level. The disturbance in the control input, $\dot{m}_{sur}(t)$ is considered throughout the system response as in (15) and the value of d_0 is considered as 10. Variation of output pressurizer level with respect to reference level for the proposed controller, the LQG-ISMC and the PI controller is shown in Fig. 25. Fig. 26 shows the deviation of output pressurizer level from the reference level for three controllers. It can be observed that the proposed controller is able to overcome the disturbance more effectively than the LQG-ISMC and the PI controller. Variation of control input is shown in Fig. 27. The plot for the sliding surface for the proposed controller is shown in Fig. 28.

4.5. Turbine speed control loop

In this control loop, objective is to maintain the mechanical power according to the demand in spite presence of uncertainties in the system. This loop is responsible for controlling the shaft speed, $\omega_{tur}(t)$ by regulating the steam flow to the turbine by adjusting the input signal to the turbine-governor valve, $u_{tg}(t)$. With this input-output combination, the relative degree of the system with respect to output is 3. Thus, similar to controller proposed in (16) in Section 4.1, for this control loop also 4-STA based controller is designed. Here, the values of μ_1 ,

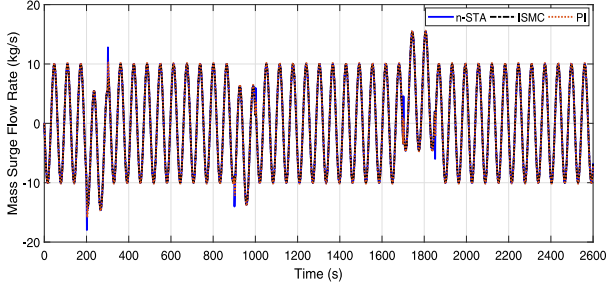


Fig. 27. Variation of input signal to CVCS system.

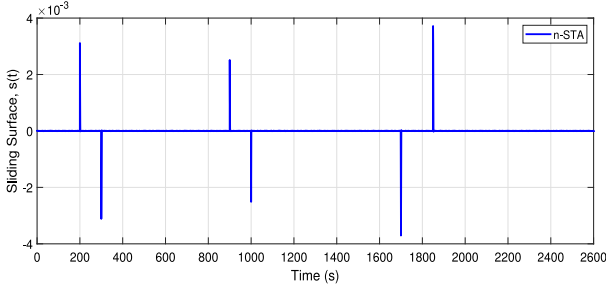


Fig. 28. Variation of sliding surface during set-point change.

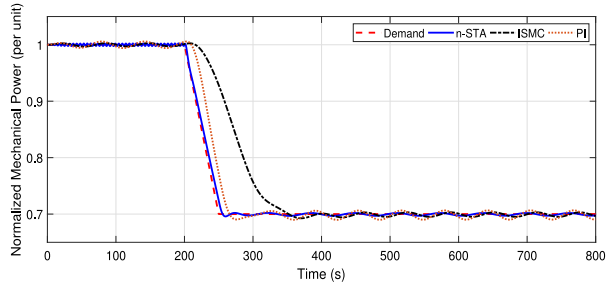


Fig. 29. Normalized mechanical power during transient.

μ_2 , μ_3 and μ_2 are selected as 1.5×10^{-2} , 1×10^{-3} , 1×10^{-2} and 1×10^3 , respectively. To design a sliding surface an error signal is defined as

$$e(t) = \omega_{tur}(t) - \omega_{tur}^{ref}(t)$$

and the values of K_P , K_D , κ_1 , and κ_2 in (3) are selected equal to 3, 8, 11 and 9, respectively. The demand power from the generator is varied as follows:

$$P_{tur}^{ref} = \begin{cases} 1, & 0 \leq t \leq 200 \\ 6 \times 10^{-3}(t - 200) + 1 & 200 < t \leq 250 \\ 0.7, & \text{elsewhere.} \end{cases}$$

In this simulation study, the controller performance is tested by varying the demand power from the generator as above in the presence of sinusoidal external disturbance. The disturbance in the control input, $u_{tg}(t)$ is considered throughout the system response as in (15) and the value of d_0 is considered as 1×10^{-2} . During this transient, the performance of the proposed controller, the LQG-ISMC and the PI controller for tracking the demand power is shown in Fig. 29. Deviation of output mechanical power from the demand power is shown in Fig. 30. It can be observed that the proposed controller follow the demand power with minimum error.

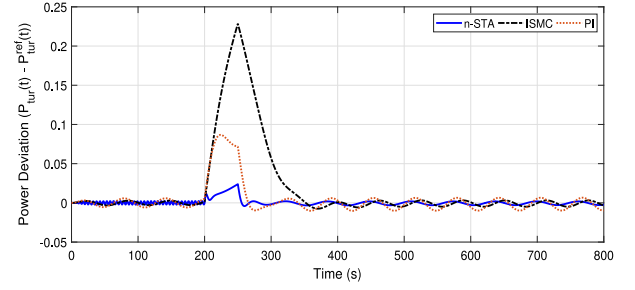


Fig. 30. Difference between demand power and normalized mechanical power during transient.

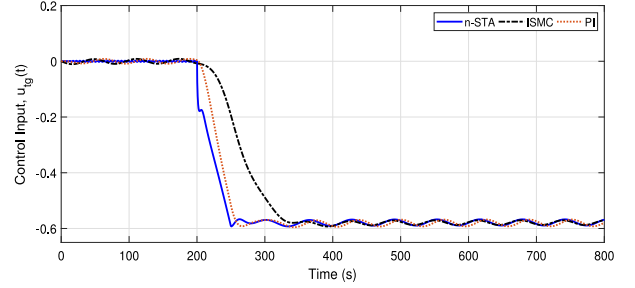


Fig. 31. Variation of input signal to turbine-governor valve.

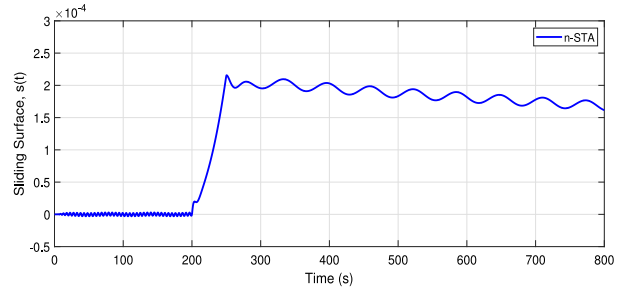


Fig. 32. Variation of sliding surface during set-point change.

5. Numerical analysis

In this section numerical analysis is performed for all the above-obtained simulation results. To show the better tracking performance to a given set-point with the proposed n-STA controller compared to the LQG-ISMC and the PI controller, the root mean squared error (RMSE) is computed. The control energy of the control input $u(t)$ is also calculated by using the 2-norm (\mathcal{L}_2 NI) method. The RMSE and \mathcal{L}_2 NI are computed as follows:

$$RMSE = \sqrt{\frac{1}{N} \sum_{i=1}^N (y_i(t) - y_{d_i}(t))^2},$$

$$\mathcal{L}_2NI = \sqrt{\sum_{i=1}^N (u_i(t))^2},$$

where $y_i(t)$ and $y_{d_i}(t)$ are the measured output and desired output signal at the i th time instant, respectively, N is the total number of samples. For simulations the sampling interval is taken as 1 ms. Ideally, smaller values of both the measures are desirable. Moreover, in case of disturbances, it is preferable that the technique should maintain the tracking performance without increasing the control efforts significantly.

The performances of the proposed n-STA, the LQG-ISMC, and the PI controller are numerically compared by calculating the RMSE and

Table 2
Performance comparison of control approaches.

Control loop	Technique	RMSE	\mathcal{L}_2 NI
Reactor power (Case-I)	n-STA	3.0402×10^{-4}	2.2530×10^0
	ISMC	1.0500×10^{-2}	1.9026×10^0
	PI	1.3200×10^{-2}	2.2629×10^0
Reactor power (Case-II)	n-STA	1.7206×10^{-4}	10.1841×10^0
	ISMC	6.8919×10^{-2}	5.9800×10^0
	PI	1.3047×10^{-2}	8.8820×10^0
Steam generator pressure	n-STA	2.1836×10^{-6}	1.7051×10^1
	ISMC	3.2559×10^{-4}	1.7039×10^1
	PI	8.8197×10^{-4}	1.7139×10^1
Pressurizer pressure by heater	n-STA	2.4356×10^{-5}	1.1311×10^7
	ISMC	2.1000×10^{-3}	8.9642×10^6
	PI	1.2452×10^{-4}	1.1463×10^7
Pressurizer pressure by spray	n-STA	2.3218×10^{-6}	7.9123×10^4
	ISMC	7.9783×10^{-4}	4.3809×10^4
	PI	7.8537×10^{-5}	8.0823×10^4
Pressurizer level	n-STA	6.6369×10^{-5}	1.1638×10^4
	ISMC	2.6891×10^{-4}	6.0208×10^3
	PI	9.6642×10^{-4}	1.1854×10^4
Turbine speed	n-STA	4.1163×10^{-3}	1.9461×10^2
	ISMC	5.2806×10^{-2}	4.1728×10^2
	PI	1.9593×10^{-2}	1.9585×10^2

the \mathcal{L}_2 NI in Table 2. It has been found that the values of RMSE for the proposed control approach are lower than those of the other two approaches. It means that the proposed n-STA controller tracks the set-point more precisely despite uncertainties and disturbances in the system. On the other hand, the ISMC spends fewer control efforts than the proposed n-STA to track the set-point. But, the LQG-ISMC is much complex control scheme compared to n-STA as the design of LQG-ISMC requires information about all the states and thus needs an observer, while the proposed controller uses only output information. Thus, it can be concluded that with the proposed controller, the complexity is reduced significantly without increasing the control efforts significantly.

6. Conclusions

In this paper, an output-feedback non-linear robust sliding mode control strategy is proposed for a pressurized water reactor type nuclear power plant. The proposed controller guarantees finite-time convergence to the reference signal for arbitrary order systems in the presence of uncertainties and external disturbances. The proposed controller is chattering free thus, it is suitable for practical applications. The effectiveness of the proposed controller to different control loops (reactor power control loop, steam generator pressure control loop, pressurizer pressure and level control loop, and turbine speed control loop) of a nuclear power plant is shown through simulation results by comparing it with well known conventional control techniques. Simulation results showed that with the proposed controller the convergence time is reduced significantly compared to integral sliding mode control and better robustness compared to the conventional proportional-integral controller in the presence of uncertainties.

As a suggestion for future work, the adaptive gain tuning law or the intelligent technique such as neural network can be used to determine the gains of n-STA which may further reduce the control efforts. In addition to that an active fault tolerant control scheme can be designed using proposed controller to accommodate different types of disturbances/faults (matched as well as mismatched) that can occur in the system.

Declaration of competing interest

The authors declare that they have no known competing financial interests or personal relationships that could have appeared to influence the work reported in this paper.

Acknowledgements

This research was funded by the Engineering and Physical Sciences Research Council (EPSRC) grant number EP/R021961/1 and EP/R022062/1.

References

- Abdulraheem, K.K., Korolev, S.A., 2021. Robust optimal-integral sliding mode control for a pressurized water nuclear reactor in load following mode of operation. *Ann. Nucl. Energy* 158, 108288.
- Abdulraheem, K.K., Korolev, S.A., Laidani, Z., 2021. A differentiator based second-order sliding-mode control of a pressurized water nuclear research reactor considering Xenon concentration feedback. *Ann. Nucl. Energy* 156, 108193.
- Ansarifar, G.R., 2016. Control of the nuclear steam generators using adaptive dynamic sliding mode method based on the nonlinear model. *Ann. Nucl. Energy* 88, 280–300.
- Ansarifar, G.R., Rafiei, M., 2015. Second-order sliding-mode control for a pressurized water nuclear reactor considering the xenon concentration feedback. *Nucl. Eng. Technol.* 47 (1), 94–101.
- Desai, R.J., Patre, B.M., Munje, R.K., Tiwari, A.P., Shimjith, S.R., 2020. Integral sliding mode for power distribution control of advanced heavy water reactor. *IEEE Trans. Nucl. Sci.* 67 (6), 1076–1085.
- Edwards, C., Spurgeon, S.K., 1998. *Sliding Mode Control: theory and Applications*. Taylor and Francis.
- Feng, Y., Yu, X., Man, Z., 2002. Non-singular terminal sliding mode control of rigid manipulators. *Automatica* 38 (12), 2159–2167.
- Filippov, A.F., 1988. *Differential Equations with Discontinuous Righthand Sides*. Springer Netherlands, Kluwer, Dordrecht, The Netherlands.
- Huang, Z., Edwards, R.M., Lee, K.Y., 2004. Fuzzy-adapted recursive sliding-mode controller design for a nuclear power plant control. *IEEE Trans. Nucl. Sci.* 51 (1), 256–266.
- Hui, J., Ling, J., Yuan, J., 2020. HGO-based adaptive super-twisting sliding mode power level control with prescribed performance for modular high-temperature gas-cooled reactors. *Ann. Nucl. Energy* 143, 107416.
- Kamal, S., Chalanga, A., Moreno, J.A., Fridman, L., Bandyopadhyay, B., 2014. Higher order super-twisting algorithm. In: 2014 13th International Workshop on Variable Structure Systems, VSS, pp. 1–5.
- Levant, A., 1993. Sliding order and sliding accuracy in sliding mode control. *Internat. J. Control* 58 (6), 1247–1263.
- Mishra, J.P., Yu, X., Jalili, M., 2016. A new class of generalized continuous robust control algorithm for arbitrary order systems. In: 2016 Australian Control Conference, AuCC, pp. 77–80.
- Moreno, J.A., Osorio, M., 2012. Strict Lyapunov functions for the super-twisting algorithm. *IEEE Trans. Automat. Control* 57 (4), 1035–1040.
- Mostafavi, S.M., Ansarifar, G.R., 2021. Pressurizer water level control with estimation of primary circuit coolant mass in nuclear power plants via robust observer based dynamic sliding mode control. *Ann. Nucl. Energy* 161, 108413.
- Munje, R.K., Patre, B.M., Tiwari, A.P., 2016. Discrete-time sliding mode spatial control of advanced heavy water reactor. *IEEE Trans. Control Syst. Technol.* 24 (1), 357–364.
- Patre, B.M., Londhe, P.S., Nagarale, R.M., 2015. Fuzzy sliding mode control for spatial control of large nuclear reactor. *IEEE Trans. Nucl. Sci.* 62 (5), 2255–2265.
- Qaiser, S.H., Bhatti, A.I., Iqbal, M., Samar, R., Qadir, J., 2009. Model validation and higher order sliding mode controller design for a research reactor. *Ann. Nucl. Energy* 36 (1), 37–45.
- Surjagade, P.V., Shimjith, S.R., Tiwari, A.P., 2020. Second order integral sliding mode observer and controller for a nuclear reactor. *Nucl. Eng. Technol.* 52 (3), 552–559.
- Utkin, V., Guldner, J., Shi, J., 2009. *Sliding Mode Control in Electro-Mechanical Systems*. CRC Press, Inc., Boca Raton, FL, USA.
- Vajpayee, V., Becerra, V., Bausch, N., Banerjee, S., Deng, J., Shimjith, S.R., John Arul, A., 2020a. Robust subspace predictive control based on integral sliding mode for a pressurized water reactor. In: 2020 7th International Conference on Control, Decision and Information Technologies, CoDIT, Vol. 1, pp. 7–12.
- Vajpayee, V., Becerra, V., Bausch, N., Deng, J., Shimjith, S.R., Arul, A.J., 2020b. Dynamic modelling, simulation, and control design of a pressurized water-type nuclear power plant. *Nucl. Eng. Des.* 370, 110901.
- Vajpayee, V., Becerra, V., Bausch, N., Deng, J., Shimjith, S.R., Arul, A.J., 2021a. Robust-optimal integrated control design technique for a pressurized water-type nuclear power plant. *Prog. Nucl. Energy* 131, 103575.
- Vajpayee, V., Top, E., Becerra, V.M., 2021b. Analysis of transient interactions between a PWR nuclear power plant and a faulted electricity grid. *Energies* 14 (6).
- Zahedi yeganeh, M.H., Ansarifar, G.R., 2018. Estimation of the poisons reactivity in the P.W.R nuclear reactors using modified higher order sliding mode observer based on the multi-point nuclear reactor model. *Ann. Nucl. Energy* 112, 158–169.
- Zare Davijani, N., Jahanfarnia, G., Esmaili Abbarian, A., 2017. Nonlinear fractional sliding mode controller based on reduced order FNPk model for output power control of nuclear research reactors. *IEEE Trans. Nucl. Sci.* 64 (1), 713–723.